# Core/Shell Bacterial Cables: A One-Dimensional Platform for Probing Microbial Electron Transfer

*Leo (Huan-Hsuan) Hsu, † Pu Deng, † Yixin Zhang, Xiaocheng Jiang**

Department of Biomedical Engineering, Tufts University, Medford, Massachusetts 02155, USA

**ABSTRACT**

Extracellular electron transfer (EET) from electrochemically active bacteria (EAB) plays a critical role in renewable bioelectricity harvesting through microbial fuel cells (MFC). Comprehensive interpretation and interrogation of EET mechanisms can provide valuable information to enhance MFC performance, which, however, are still restricted by the intrinsic complexity of natural biofilm. Here, we design core/shell EAB-encapsulating cables as a one-dimensional model system to facilitate EET studies, where the local microenvironments can be rationally controlled to establish structure-function correlations with full biological relevance. In particular, our proof-of-concept studies with *Shewanella loihica* PV-4 (*S. loihica*) encapsulating cables demonstrate the precise modulation of fiber diameters (from 6.9±1.1 μm to 25.1±2.4 μm) and bacteria interactions, which are found to play important roles in programming the formation of different inter-cellular structures as revealed by in-situ optical and ex-situ electron microscopic studies. As-formed bacterial cables exhibit conductivity in the range of 2.5 to 16.2 $mS \cdot cm^{-1}$, which is highly dependent on the bacteria density as well as the nature and number of intercellular interconnections. Under

electron-acceptor limited conditions, the closely contacted bacteria promote the development of high density self-assembling nanomaterials at cellular interfaces which can be directly translated to the increase of EET efficiency (16.2 $mS \cdot cm^{-1}$) as compared with isolated, remotely-connected bacteria samples (6.4 $mS \cdot cm^{-1}$). Introducing exceeding concentrations of soluble electron acceptors during cell culture, however, substantially suppresses the formation of cellular interconnections and leads to significantly reduced conductivity (2.5 $mS \cdot cm^{-1}$). Frequency-dependent measurements further revealed EET of EAB networks shared similar characteristics to electron hopping in conductive polymer matrix, including dominant DC-conduction in the low frequency region, and AC induced additional electron hopping when the applied frequency is above the critical frequency ($10^5$ Hz). The current work represents a strategically new approach for non-invasively probing EET with rationally defined micro-environment and cellular interactions across a wide range of length scales, which is expected to open up new opportunities for tackling the fundamentals and implications of EET.

**KEYWORDS**

Extracellular Electron Transfer, Microbial Nanowire, Microbial Fuel Cell, Cytochromes, Shewanella, Alginate

**MAIN TEXT**

As a promising technology for sustainable energy production, microbial fuel cells (MFCs) have attracted increasing interests due to their capabilities to directly transform various organic substrates into electricity under resource limited conditions.[1] However, the low power density of MFCs has limited their applications to date.[2] Extracellular electron transfer (EET), the process that directly transfers metabolic electrons from electrochemically active bacteria (EABs) to external

electrodes without intervening catalysts serves as the basis for electricity production in MFCs.[1,3,4] Understanding mechanisms and limitations of EET is critical to define and potentially-improve power output of MFCs. Recently, researchers discover that EETs in two model EAB species, *Shewanella* and *Geobacter*, are mainly associated with their surface membrane proteins – c-type cytochromes (cyts).[3,5] These cyts allow direct electron transfer from one bacterium to another or from bacteria to solid electron acceptors when they are closely contacted. More interestingly, EABs can also form a variety of micro- to nano- structures to enable longer range EET. For example, EABs protrude conductive pilus-like nanostructures – often known as microbial nanowires – from bacteria surfaces which serve as alternative electron transfer pathways to extend the EET distance and maximize transport efficiency.[6,7] It has also been reported that some marine microbes can fuse surface membranes to generate centimeter-long "bacteria cables" to transfer their metabolic electrons from the bottom nutrient-rich layer to the surface oxygen-rich layer.[8] While significant progress has been made in the EET studies, the complex nature of native biofilms limited the unambiguous investigation of EET mechanisms and the relationship between these conductive structures with corresponding functions.[9–11] These limitations lead to vague and actively debated EET mechanisms such as metallic like EET process vs electron hopping.[11–14]

Recent developments of nanotechnology-enabled platforms allow the real-time probing of EET from "bottom-up".[15,16] In particular, nanostructured electrodes, in which the presence or absence of cell/electrode contacts can be physically controlled, have been developed so that the contribution from direct or mediated electron transfer could be unambiguously distinguished. Combined with high-resolution in-situ imaging, the correlation between current output and microbe/electrode interaction has been demonstrated at the single-cell level. The current generation from single bacterium not in biofilms establishes the intrinsic limit of MFC current

density, ~$10^6$ A/$m^3$,[15] which is 2-3 orders of magnitude higher than the best value reported in working MFCs.[17] These results indicate that the performance of state-of-the-art MFCs is not intrinsically limited by EAB or EAB/electrode interface and highlight the great potential of this burgeoning technology. To scale up single-EAB performance to the entire cell population and further improve power density, there is a strong need to further extend the bottom-up EET studies to elucidate the fundamental mechanism and structure-function correlations in the context of cell-cell interactions. Toward this goal, we have created an artificial extracellular matrix to engineer EAB biofilm from the bottom-up. Specifically, core/shell hydrogel fibers were designed and developed for live EAB encapsulation/confinement which allows rationally-controlled microenvironments and bacterium-bacterium interactions. These bacteria networks represent 1D model systems to investigate EET with minimal invasiveness, full biological relevance, and across multiple length scales.

The 1D bacterial fiber is generated through a two-stage flow focusing device consisted of coaxially-aligned glass capillaries with multiple fluidic inlets (**Figure 1a**).[18] The glass capillaries with diameters of 30 and 60 μm are exploited at the first and second stage of the device, respectively. During operation, bacterium solution first flows through the 30 μm capillary with flow rate at 0.2 mL/hr. This bacteria flow is focused into a micrometer-scale stream before entering the second capillary where 2% alginate solution is injected as the shell flow. Alginate is exploited as the 1D scaffolding for bacteria encapsulation and confinement, because of its structural similarity to polysaccharide matrices in native biofilms, desirable porosity for efficient nutrients/metabolites exchange, and easy degradation via a variety of chemical approaches.[19] After exiting the second capillary, this core-shell flow interacts with a "sheath" flow containing 100 mM $CaCl_2$, the alginate crosslinking reagents, which crosslinks alginate to become a solid hydrogel.

**Figure 1b and c** show fluorescent images (taken under low and high magnifications) of bacteria/alginate core/shell fibers generated when flow rates of alginate shell and $Ca^{2+}$ sheath are controlled at 0.9 mL/hr and 200 mL/hr, respectively. As measured from random locations of **Figure 1b**, this flow focusing device can consistently generate core–shell fibers with narrow core size distributions (11.6 ± 0.68 um) (**Figure 1b inset**).

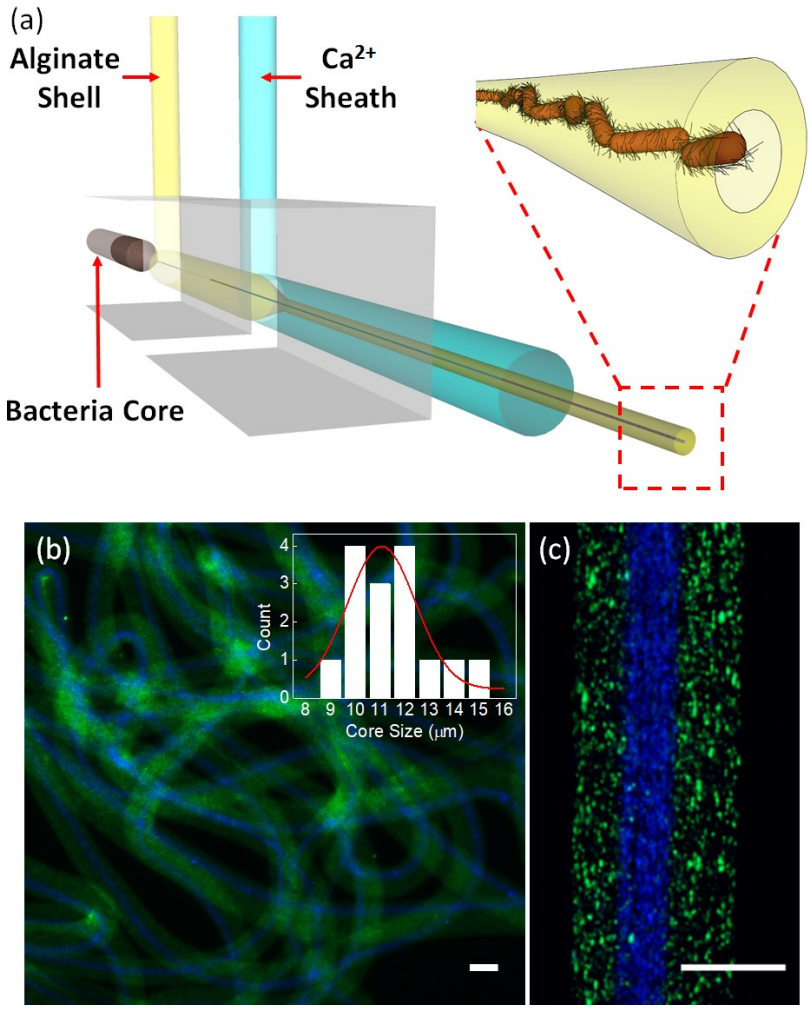


**Figure 1. Microfluidic generation of core/shell bacterial cables.** (a) Schematics of the two-stage flow focusing device for core/shell bacterial fiber generation. The EAB-containing core stream (brown) is flow focused before entering the alginate shell stream (yellow). The core/shell hydrogel fiber is formed at the end of the device when a $CaCl_2$ sheath flow is introduced to

crosslink the alginate; (b, c) Low- (b) and high-magnification (c) fluorescent images of as-fabricated core/shell fibers; green color indicates the alginate shell mixed with Dextran nanoparticles and blue indicates the bacteria with Hoechst nuclei staining. Scale bars: 50 μm (b) and 25 μm (c)

The two-stage flow focusing microfluidic device enables a unique possibility to precisely modulate the fiber structure and bacteria density as a strategy to control cellular interactions and microenvironment in 1D. By changing the first-stage flow rate from 0.4 mL/hr to 0.1 mL/hr, the diameter of the "bacteria core" can be effectively reduced from $25.1 \pm 2.4$ μm to $6.9 \pm 1.1$ μm (**Figure 2a, b**). Particularly, at 0.1 mL/hr core flow rate, single stream of bacteria can be focused/aligned in the fiber core which is approaching the real 1-D regime (**Figure 2aIV**). The modulation of the shell flow rate can provide additional control of the fiber geometry,[20] with the increase of shell flow rate leading to the reduction of core diameter. Additionally, the density of the encapsulated bacteria can also be modulated by varying the stock concentration of the bacteria core flow. This allows us to rationally tune cellular interactions, where the bacteria could be in close contact or isolated with designed spacing (**Figure 2c**), thus offering the possibility to rationally program the structure and properties of bacterium-bacterium interconnections when forming the 1D EAB network.

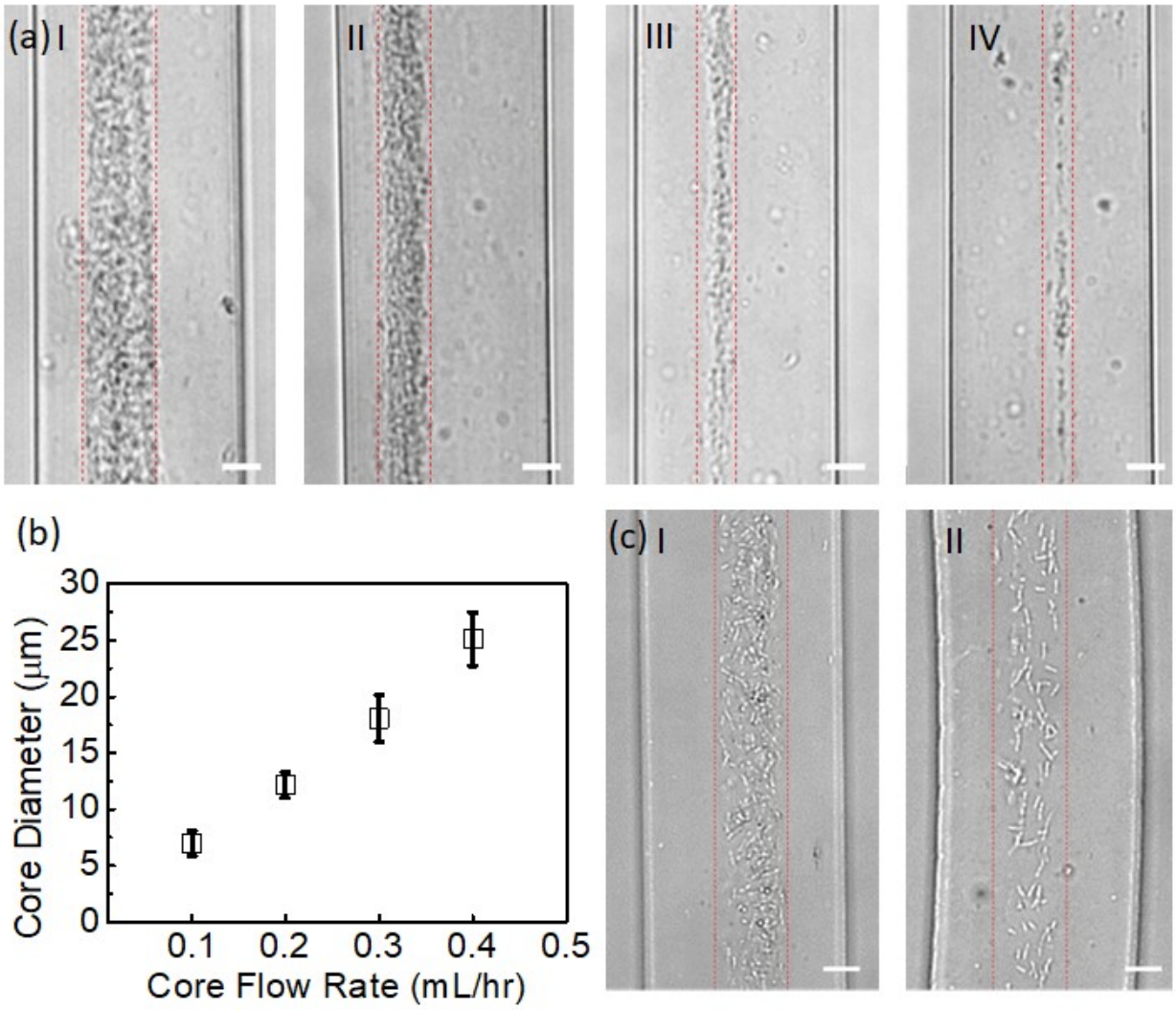


**Figure 2. Modulations of cell-cell interactions within the core/shell fibers** (a) Bright-field images of bacterial cables with varied core diameters. Core flow rate: (I) 0.4mL/hr; (II) 0.3mL/hr; (III) 0.2mL/hr (IV) 0.1mL/hr. (b) Summary of the core size distribution at different flow rates. n=10 (c) Bright-field images of bacterial cables with high (I) and low (II) bacteria density. Scale bar: 10 μm

As-generated bacteria cables are collected and subject to systematic culture tests under controlled environments,[21] where effects of initial EAB density and culture conditions on the structure and morphology of 1D cellular interconnections are examined with both optical and electron microscopy.[22] Confocal fluorescent images of high-density bacterial cables cultured under

electron acceptor limited conditions revealed that the compact encapsulation of bacteria promotes the formation of cable-like structure (**Figure 3a**), where the outer membrane of cells are closely connected together, sharing very similar morphology to the filamentous bacteria observed in nature.[8] In order to further investigate the nanoscale interfaces within the structure, the alginate shell of the bacterial cable is gently removed with calcium chelating reagents[23] and the exposed bacteria-derived structures are analyzed under the scanning electron microscope (SEM). The SEM images have revealed two types of "nanowires" that are generated in this 1D bacterial network (**Figure 3d**). Type-I nanowires are few micrometers in length and tens of nanometers in width and are bridging isolated EAB. These nanowires are morphologically consistent with earlier studies which demonstrated them as membrane extensions.[6,24] Type-II "nanowires" or pili, which are generally <100 nm, distributes at the membrane connections of bacteria with notably higher density as compared with Type-I nanowires (**Figure 3d inset**). We hypothesize these nanostructures have a similar role in electron transfer as the "ridges" observed in natural bacteria cable, which could eventually fuse with connected bacteria.[8] In contrast, in low density EAB network, the isolated cell bodies limited the formation of bacteria cable as shown in the confocal fluorescent image (**Figure 3b**). No clear connections between bacteria bodies can be observed in majority of this network except a few bacteria filamentous structure extending from outer membranes (red arrows in **Figure 3b**). A detailed characterization of these nanoscale structures under SEM showed similar morphologies to the Type-I nanowires in the high-density EAB networks (**Figure 3e**). No Type-II nanowires have been observed in low EAB density networks, indicating the importance of initial cell density/cell-cell interaction in directing the formation of these short-range inter-cellular structures.

Furthermore, to understand the influence of local electron acceptors on the development of bacterial interconnections, a separated experiment is carried out where the high density bacterial cables are cultured under electron acceptor (fumarate) rich condition. Fumarate can easily access EAB through diffusion which triggers alternative metabolic pathways such as cyts-enzyme interactions[25] and electron tunneling through surface protein,[6] thus suppressing the nanowire formation as confirmed by both fluorescent and SEM characterizations (**Figure 3c and f**). Only a very small amount of pilus-like structures have been observed under SEM (**Figure 3f**) which interconnect adjacent bacteria (< 500 nm separation) and form a loose network. These low-density nanowires cannot provide sufficient structural support; hence, this network was broken into separated bacteria after the removal of alginate shell.

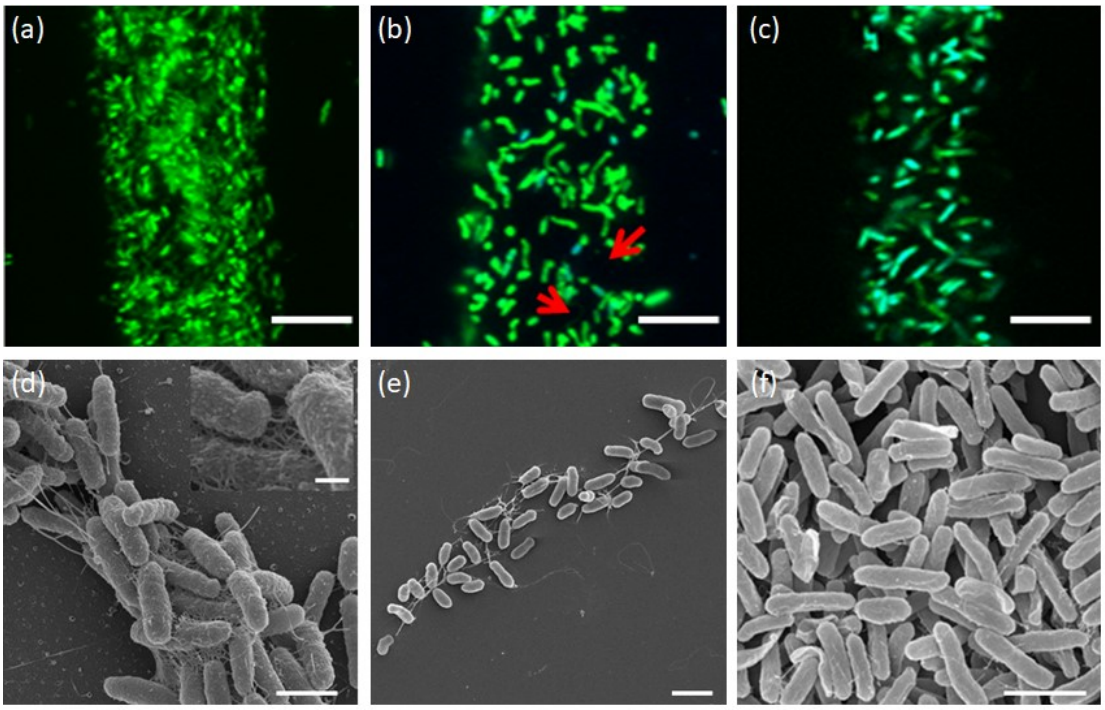


**Figure 3. Fluorescence and SEM characterizations of the 1D bacterial networks**. *Confocal fluorescent images* of bacteria cables with high (a) and low (b) EAB density; as well as the high EAB density fiber cultured under electron acceptor rich condition conditions (c). Scale bar: 10 μm.

*High magnification SEM images* of high (d) and low (e) EAB density networks as well as high density networks cultured under electron acceptor rich condition conditions (f). Scale bars: 1 μm (d); 1.5 μm (e), and 2 μm (f).

The electrical properties of as-fabricated bacterial cables are investigated with both DC current-voltage (I-V) and frequency-dependent AC conductivity measurement.[26] All measured bacterial cables showed linear I-V relationships (**Figure 4a inset**), indicating that the current vs potential change is mostly attributed to the EET process with minimal electrochemical reaction at electrode interface. The conductivity of each sample is calculated from the I-V measurements and summarized in **Figure 4a**. The bacterial cables with high density networks exhibit higher conductivity ($16.2 \pm 4.2$ mS·cm$^{-1}$) as compared with low density ($6.4 \pm 1.6$ mS·cm$^{-1}$) networks. These results suggest that the EET efficiencies can be enhanced by increasing bacteria density in the fibers which can promote generations of membrane contact and high-density nanowires (**Figure 3a, d**) thus introduce additional EET pathways. The very low conductivities of bacterial networks cultured under electron acceptor rich conditions ($2.5 \pm 0.5$ mS·cm$^{-1}$) further confirm that bacterial interconnections are the key factors in long range EET. Reduction of bacterial interconnections due to high concentration electron acceptors restricts the development of long range EET pathway; thus, results in a low EET efficiency.

The frequency-dependent impedance measurement is performed in the range of 0.1 Hz to$10^6$ Hz with potential set at 0 V (**Figure 4b).** The key features are in good consistence with an electron hopping mechanism in conductive polymers.[27] In the low frequency range of 100 mHz to $10^5$ Hz, EET is dominated by the resistance of bacterial network which is determined by the intrinsic macroscale connection of the whole bacterial network. As frequency raises over the critical frequency ($10^5$ Hz), the applied AC potential enables additional electron hopping processes

thus further reducing the impedance.[27] This transition from DC to DC+AC EET mechanisms is also reflected from the phase angle shift (**Figure 4b**), which stays constant at 0º between 100 mHz to $10^5$ Hz then progressed to -80º along with the increase of frequency. It's worth noting that our current frequency-dependent impedance measurement along bacterial cables differs significantly from conventional electrochemical impedance spectroscopy (EIS) studies of EAB biofilms. This measurement is dominated by the EET within the centimeter-long 1D channel with minimal contribution from EAB/electrode interfaces. By further improving electrical interface between inorganic electrodes and EABs (*e.g.*, through biogenic production of metal/semiconductor nanoparticles[3] that are intimately coupled with redox centers), the platform has the potential to tackle EET mechanisms and limitations that are intrinsic to bacterial networks.

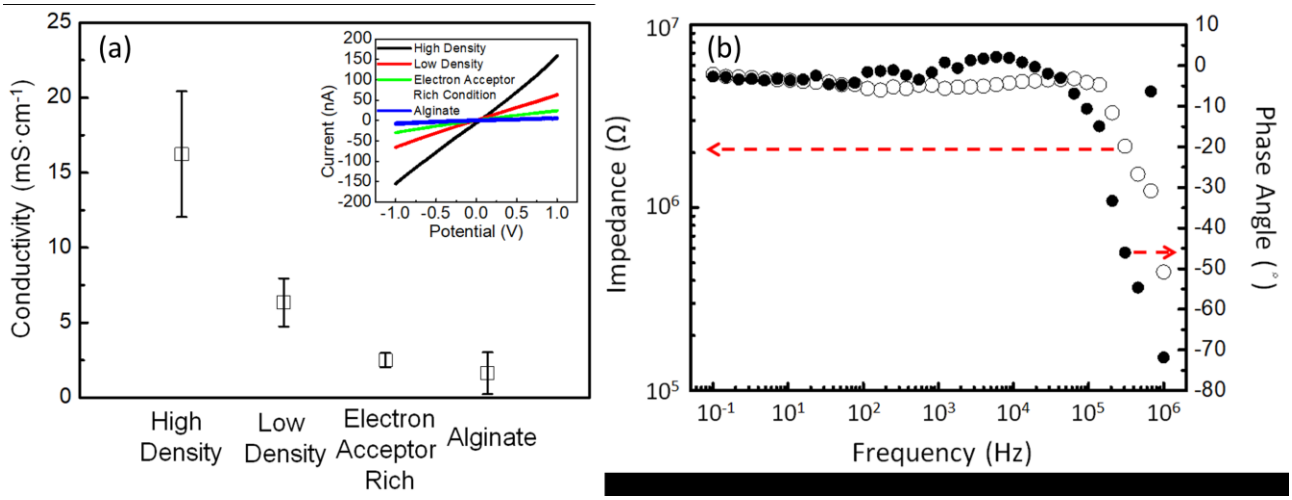


**Figure 4. Electrical properties of bacteria cables.** (a) Conductivities of high density, low density, electron acceptor rich condition, and pure alginate fiber control derived from the I-V characteristics. Conductivities were calculated based 2 cm in fiber length and 50 μm in fiber diameter Inset: I-V characteristics of correspondent bacterial cable samples. n=3 (b) Frequency-dependent impedance measurement of high density network. Black and white marks represent

the impedance and phase angle shift measurements as the response of frequency changes, respectively.

In conclusion, we have demonstrated the development of EAB-encapsulated core/shell fibers as 1D model system to investigate EET across different length scales with rationally designed bacterial interconnections. This platform allows precise modulation of the cell-cell interactions from closely membrane contact to fully isolated, as well as local microenvironments from electron receptor limited to electron receptor rich conditions. These modulations lead to significant effects in both structural (from isolated bacteria to high density nanowire connections) and electrical properties (from 2.5 to 16.2 $mS \cdot cm^{-1}$) of these 1-D bacterial networks. This unique capacity can open up a new possibility to in-situ non-invasive investigation of EET in the living EAB network which is anticipated to overcome challenges present in the current studies in native biofilms and provide explicit insights of EET mechanisms. The fundamental understanding of structure-function relationship in the context of cell-cell interactions will also facilitate the design and development of novel MFC systems with rationally designed EET pathways. In particular, these bacteria cables naturally serve as 1D building blocks to construct hierarchical anode structures from the bottom-up, in which both charge and mass transport can be effectively optimized at single-fiber and ensemble levels to maximize the MFC performance.

## AUTHOR INFORMATION


### Corresponding Author

*Email: Xiaocheng.Jiang@tufts.edu


### Author Contributions

Leo (Huan-Hsuan) Hsu[†] and Pu Deng[†], contributed equally to this work.

## ACKNOWLEDGMENT

This study was supported by National Science Foundation (NSF DMR- 1652095) and NSERC Postdoctoral Fellowships Program (PDF-487877-2016).

## REFERENCES

(1) Logan, B. E.; Hamelers, B.; Rozendal, R.; Schröder, U.; Keller, J.; Freguia, S.; Aelterman, P.; Verstraete, W.; Rabaey, K. *Environ. Sci. Technol.* **2006**, *40* (17), 5181–5192.

(2) Jiang, X.; Hu, J.; Lieber, A. M.; Jackan, C. S.; Biffinger, J. C.; Fitzgerald, L. A.; Ringeisen, B. R.; Lieber, C. M. *Nano Lett.* **2014**, *14* (11), 6737–6742.

(3) Kumar, A.; Hsu, L. H.-H.; Kavanagh, P.; Barrière, F.; Lens, P. N. L.; Lapinsonnière, L.; Lienhard V, J. H.; Schröder, U.; Jiang, X.; Leech, D. *Nat. Rev. Chem.* **2017**, *1*, 24.

(4) Schröder, U. *Phys. Chem. Chem. Phys.* **2007**, *9* (21), 2619–2629.

(5) Shi, L.; Richardson, D. J.; Wang, Z.; Kerisit, S. N.; Rosso, K. M.; Zachara, J. M.; Fredrickson, J. K. *Environ. Microbiol. Rep.* **2009**, *1* (4), 220–227.

(6) Pirbadian, S.; Barchinger, S. E.; Leung, K. M.; Byun, H. S.; Jangir, Y.; Bouhenni, R. A.; Reed, S. B.; Romine, M. F.; Saffarini, D. A.; Shi, L.; et al. *Proc. Natl. Acad. Sci. U. S. A.* **2014**, *111* (35), 12883–12888.

(7) Reguera, G.; McCarthy, K. D.; Mehta, T.; Nicoll, J. S.; Tuominen, M. T.; Lovley, D. R. *Nature* **2005**, *435* (7045), 1098–1101.

(8) Pfeffer, C.; Larsen, S.; Song, J.; Dong, M.; Besenbacher, F.; Meyer, R. L.; Kjeldsen, K. U.; Schreiber, L.; Gorby, Y. A.; El-Naggar, M. Y.; et al. *Nature* **2012**, *491*, 218.

(9) Malvankar, N. S.; Rotello, V. M.; Tuominen, M. T.; Lovley, D. R. *Nat. Nanotechnol.* **2016**, *11* (11), 913–914.

(10) Yates, M. D.; Strycharz-Glaven, S. M.; Golden, J. P.; Roy, J.; Tsoi, S.; Erickson, J. S.; El-Naggar, M. Y.; Barton, S. C.; Tender, L. M. *Nat. Nanotechnol.* **2016**, *11* (11), 910–913.

(11) Malvankar, N. S.; Vargas, M.; Nevin, K. P.; Franks, A. E.; Leang, C.; Kim, B.-C.; Inoue, K.; Mester, T.; Covalla, S. F.; Johnson, J. P.; et al. *Nat. Nanotechnol.* **2011**, *6* (9), 573–579.

(12) Pirbadian, S.; El-Naggar, M. Y. *Phys. Chem. Chem. Phys.* **2012**, *14* (40), 13802–13808.

(13) Strycharz-Glaven, S. M.; Snider, R. M.; Guiseppi-Elie, A.; Tender, L. M. *Energy Environ. Sci.* **2011**, *4* (11), 4366.

(14) Malvankar, N. S.; Tuominen, M. T.; Lovley, D. R. Energy Environ. Sci., 2011, 4, 4366. *Energy Environ. Sci.* **2012**, *5*, 6247–6249.

(15) Jiang, X.; Hu, J.; Petersen, E. R.; Fitzgerald, L. a; Jackan, C. S.; Lieber, A. M.; Ringeisen, B. R.; Lieber, C. M.; Biffinger, J. C. *Nat. Commun.* **2013**, *4* (May), 2751.

(16) Jiang, X.; Hu, J.; Fitzgerald, L. A.; Biffinger, J. C.; Xie, P.; Ringeisen, B. R.; Lieber, C. M. *Proc. Natl. Acad. Sci.* **2010**, *107* (39), 16806–16810.

(17) Xie, X.; Criddle, C.; Cui, Y. *Energy Environ. Sci.* **2015**, *8* (12), 3418–3441.

(18) The two-stage flow focusing device is assembled with two glass capillaries with tip diameters of 30 (1st stage) and 60 (2nd stage) μm. During fabrication, the 1st stage capillary is inserted 1 cm into the inlet of 2nd stage capillary and carefully aligned to the center. The 1 cm insertion is critical to avoid undesired turbulences when forming bacteria/alginate core/shell stream. During operation, the first capillary will focus the bacteria flow into a micrometer-scale stream before entering the second capillary where 2% alginate solution will be injected as the shell flow. The flow rates of both bacteria and alginate are delicately controlled in a low Reynolds number regime to avoid the occurrence of turbulence flow which may lead to the mixing of two streams. After exiting the second capillary, this core/shell stream will interact with a "sheath" flow containing alginate crosslinking reagents

(such as $Ca^{2+}$ or $Ba^{2+}$), where the gelation will occur at the alginate/sheath flow interface to form the bacteria/alginate core/shell fibers.

(19) Lee, K. Y.; Mooney, D. J. *Prog. Polym. Sci.* **2012**, *37* (1), 106–126.

(20) Onoe, H.; Okitsu, T.; Itou, A.; Kato-Negishi, M.; Gojo, R.; Kiriya, D.; Sato, K.; Miura, S.; Iwanaga, S.; Kuribayashi-Shigetomi, K.; et al. *Nat. Mater.* **2013**, *12*, 584.

(21) Culture of *S. loihica* PV-4 was based on previous reference.[2] In general, bacteria grown from −80 °C glycerol stock were inoculated in 50 mL of Luria−Bertani (LB) broth with gentle shaking (100 rpm) in air for 48 h at 25 °C. After centrifuged at 4000 rpm for 20 min, the isolated bacteria were redispersed in minimal media (MM) containing 30 mM sodium lactate. The formulation of MM was reported previously.[24] The redispersed culture was shaken (100 rpm) in air 24h at 25 °C for cable fabrication. High density bacteria cables were generated by applying bacteria solution with OD=24 as core flow (flow rate 0.2ml/h), while low density bacteria cables were fabricated with OD=5 bacterium solution (flow rate 0.2ml/h). Each cable samples were cultured in a PDMS chamber filled with MM where generated an electron acceptor-limited condition. Additionally, MM with 40 μM fumarate (Sigma-Aldrich) was used to culture the electron acceptor-rich sample. After two days culture, all the fibers were collected for image taking and electrical measurement.

(22) Samples for fluorescence imaging were prepared as follows: Bacterial nuclei were stained by 30x diluted Hoechst 33342 (Fisher Scientific). Bacterial surface protein were then stained by 200x diluted Syproorange (Fisher Scientific). Stained samples were fixed with 2% paraformaldehyde for 1h at room temperature. Fluorescence images were carried out with Leica FLIM SP8 confocal microscope. Samples for SEM study were prepared by following steps: Cable samples were fixed in 2% glutaraldehyde solution (1h, room temperature). After DI water rinsing, the samples were dehydrated in series of ethanol solutions (50, 75, 90, 95, 100% and 100%, 10 min each). Dehydrated samples were then critical point dryed (Leica EM CPD300), and sputtered with Pd/Pt alloy. Images were acquaired with Zeiss Ultra 55 SEM.

(23) Strand, B. L.; Mørch, Y. A.; Skjåk-Bræk, G. *Minerva Biotecnol.* **2000**, *12* (4), 223–233.

(24) Gorby, Y. A.; Yanina, S.; McLean, J. S.; Rosso, K. M.; Moyles, D.; Dohnalkova, A.; Beveridge, T. J.; Chang, I. S.; Kim, B. H.; Kim, K. S.; et al. *Proc. Natl. Acad. Sci. U. S. A.* **2006**, *103* (30), 11358–11363.

(25) Schwalb, C.; Chapman, S. K.; Reid, G. A. *Biochemistry* **2003**, *42* (31), 9491–9497.

(26) DC I-V and AC EIS measurements were performed by Biologic SP200 Potentiostat. To establish electrical contact, as-fabricated fibers were deposited onto a pair gold electrodes with 20 mm separation. Carbon nanotube paste was then applied at the electrode/fiber interface to further improve the electric interconnections. The measurements were performed after rinsed the fibers with MM, DI water (7 times) and 100% ethanol.

(27) Papathanassiou, A. N.; Sakellis, I.; Grammatikakis, J. *Appl. Phys. Lett.* **2007**, *91* (12), 2005–2008.

**Table of Contents Graphic**